Host–Guest Systems

International Edition: DOI: 10.1002/anie.201702926
German Edition: DOI: 10.1002/ange.201702926

Renewable Molecular Flasks with NADH Models: Combination of Light-Driven Proton Reduction and Biomimetic Hydrogenation of Benzoxazinones

Liang Zhao, Jianwei Wei, Junhua Lu, Cheng He, and Chunying Duan**

Abstract: *Using small molecules with defined pockets to catalyze chemical transformations resulted in attractive catalytic syntheses that echo the remarkable properties of enzymes. By modulating the active site of a nicotinamide adenine dinucleotide (NADH) model in a redox-active molecular flask, we combined biomimetic hydrogenation with in situ regeneration of the active site in a one-pot transformation using light as a clean energy source. This molecular flask facilitates the encapsulation of benzoxazinones for biomimetic hydrogenation of the substrates within the inner space of the flask using the active sites of the NADH models. The redox-active metal centers provide an active hydrogen source by light-driven proton reduction outside the pocket, allowing the in situ regeneration of the NADH models under irradiation. This new synthetic platform, which offers control over the location of the redox events, provides a regenerating system that exhibits high selectivity and efficiency and is extendable to benzoxazinone and quinoxalinone systems.*

Catalytic synthetic methods that are inspired by natural enzyme prototypes that react under an ambient atmosphere and use benign solvents and clean energy are a major endeavor in synthetic chemistry.[1] To match the efficiency and selectivity of enzymatic systems, chemists use small molecules with defined hydrophobic cavities that emulate the properties of enzyme active sites to catalyze specific chemical transformations.[2,3] An exciting area in this research includes the incorporation of transition-metal moieties as redox-active vertices that mimic the highly evolved and finely tuned natural photocatalytic systems by catching organic dyes in the pocket.[4,5] Such a separation of the redox events by the inner and outer spaces of the cavity provides a new synthetic platform that combines photocatalytic reduction with a specific hydrogenation reaction.

Nature has developed millions of redox systems in which the redox process is catalyzed by numerous coenzymes.[6,7] Taking advantage of modified prototypes and hydride reduction cofactors, chemists have developed a biomimetic hydrogenation approach employing Hantzsch esters with relevant compounds that function as mimics of nicotinamide adenine dinucleotide (NADH).[8,9] In terms of the availability, atom economy, and by-product removal, the combination of light-driven proton reduction to regenerate the active sites is a promising approach that has not been reported in the field of renewable and recyclable NADH mimics.[10,11] From a catalytic perspective, the challenges in developing one-pot catalytic processes include the combination of photoredox catalysis and hydrogenation catalysis, in addition to the compatibility between the dynamic kinetics and reaction intermediates and the synergy of the inside and outside redox processes.

Through direct modulation of two tridentate chelating donors at the *meta* sites of a central dihydropyridine amido (DHPA) mimic relative to the active site of an NADH model, metal-organic macrocycles that contain redox-active nickel(II) nodes for photocatalytic proton reduction and renewable active sites of a NADH model system for the hydrogenation of benzoxazinones were prepared (Scheme 1), and their catalytic performance was evaluated. We envisioned that the modified pocket in the molecular flask would strongly interact with substrates that will then react with the active sites of the NADH mimics to produce the hydrogenation product and NAD^+ mimics in the inner space of the pocket. Redox-active metal centers provide the possibility of photocatalytically reducing protons,[12] forming active H-atoms that interact with the NAD^+ mimics, and regenerating the active sites for another cycle. Controlling the location of the reaction cycles could be a promising approach to provide reactions

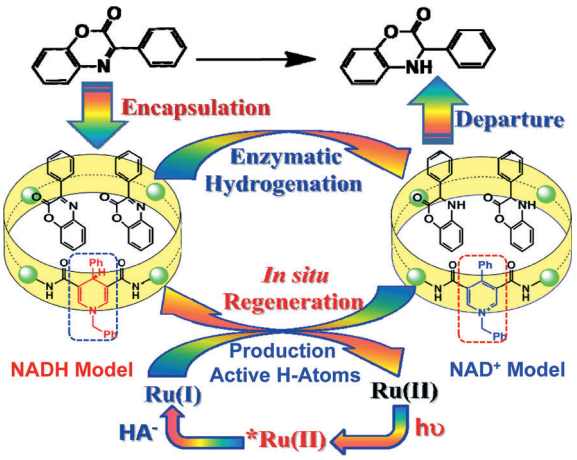

Scheme 1. Schematic of the redox-active macrocycle with NADH mimics showing the combination of biomimetic hydrogenation and in situ regeneration of active sites through photocatalytic reduction in a one-pot process.

[*] Dr. L. Zhao, J. Wei, J. Lu, Prof. C. He, Prof. C. Duan
State Key Laboratory of Fine Chemicals, Dalian University of Technology
Dalian, 116024 (China)
E-mail: hecheng@dlut.edu.cn
cyduan@dlut.edu.cn

Supporting information for this article can be found under: https://doi.org/10.1002/anie.201702926.

with sufficient compatibility between the kinetics and reaction intermediates.

The ligand H_2**ZPB**, which contains a central DHPA backbone relative to the active site of the NADH model, was synthesized by a Schiff-base reaction of 2-pyridylaldehyde and 1-benzyl-4-phenyl-1,4-dihydropyridine-3,5-dicarbohydrazide. The reaction of the $Ni(ClO_4)_2$ and the H_2**ZPB** gives the redox-active macrocycle Ni-**ZPB**. Single-crystal structure analysis revealed the formation of a tetranuclear macrocycle with four central DHPA moieties. The macrocycle Ni-**ZPB** is positioned on a C_2 axis through the connection of four ligands and four redox-active nickel ions in an alternating fashion (Figure 1).[13] The edges of the tetragon formed by the

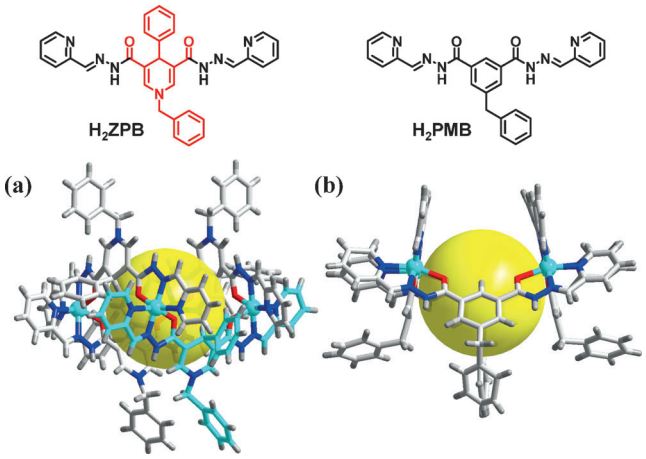

Figure 1. Structures of the molecular macrocycles Ni-**ZPB** and Ni-**PMB**, showing the coordination geometry of the ions and the direction of the active site of the H_2**ZPB** ligands. Nickel = cyan, oxygen = red, nitrogen = blue, carbon = white, and hydrogen = grey.

NADH-mimicking ligands that linearly bridge two metal ions create an average Ni···Ni separation of circa 8.62 Å, suggesting that the cavity of the macrocycle is sufficiently large to encapsulate planar aromatic substrates. Each nickel ion was coordinated in a *mer* position with a pair of delocalized N_2O chelators to modify the redox potential to a region suitable for electrochemical reduction of the proton. The DHPA moieties on parallel edges of the macrocycle are positioned on the same side, with another pair of DHPA moieties above or beneath the macrocycle and with active sites positioned in the interior of the pocket. These amide groups are located around the charged pocket, providing enriched hydrogen bonding triggers for the recognition and activation of substrate encapsulation.[14] The close proximity between the encapsulated substrate and active sites facilitates a direct H-transfer reaction from the cofactor mimics to the substrate located within the inner space of the pocket, ensuring size and shape selectivity associated with the confining effects of the molecular flask.[15]

The stability of Ni-**ZPB** in solution was characterized by ESI-MS analysis. Intense peaks at $m/z = 599.15$, 624.14, and 649.13 are assigned to $[Ni_4(H\mathbf{ZPB})_4]^{4+}$, $[Ni_4(H\mathbf{ZPB})_3(H_2\mathbf{ZPB})\cdot ClO_4]^{4+}$, and $[Ni_4(H\mathbf{ZPB})_2(H_2\mathbf{ZPB})_2\cdot 2\,ClO_4]^{4+}$, respectively. Upon addition of, 3-phenyl-2*H*-1,4-benzoxazin-2-one (Substrate **1**), ESI-MS spectra exhibited a new peak at $m/z = 568.75$ assigned to $[Ni_4(H\mathbf{ZPB})_3(H_2\mathbf{ZPB})(\mathbf{1})_2]^{5+}$ (Supporting Information, Figure S3), suggesting the formation of a 1:2 stoichiometric host–guest species. Microcalorimetric titration[16] of host–guest complexation in the polar solvent DMF with a higher solubility was carried out, revealing a good n value of 2.0 from the curve fitting using the "independent" model (Supporting Information, Figure S11), corresponding to enthalpy (ΔH) and entropy ($T\Delta S$) changes for Ni-**ZPB**⊃(**1**)$_2$ of -0.49 ± 0.03 and 29.2 kJ mol^{-1}, respectively. The host–guest complexation species and the active sites of NADH mimics are the basis for the biomimetic hydrogenation within the pocket of macrocycle.

The evaluation of catalytic reactions first focused on the hydrogenation of benzoxazinones. For a solution containing **1** and Ni-**ZPB** as the NADH mimics, the conversion reached 95% (racemates, no further separation for the two enantiomers) in the presence of ascorbic acid (**H_2A**). Using the salt $Ni(ClO_4)_2$ or **H_2A** alone gave a trace amount of the product, and loading an identical amount of the ligand itself yielded only a small amount of product. A control experiment using a benzoxazinone with bulky substituents, **2**, 3-(4′-(tert-butyl)-[1,1′-biphenyl]-4-yl)-6-(4-(tert-butyl)phenyl)-2*H*-1,4-benzoxazin-2-one, with a size larger than that of the pocket of Ni-**ZPB**, yielded 17% of product under the same conditions. Clearly, compound Ni-**ZPB** is responsible for the biomimetic hydrogenation reaction, providing an efficient and confined space for size or shape selectivity (Supporting Information, Figure S18).[17]

The active sites of the NADH mimics in the macrocycle could be regenerated by adding reducing agents.[18] In the presence of $Na_2S_2O_3$ as a reducing agent, a loading of 0.1% mol ratio of Ni-**ZPB** resulted in 96% conversion for the hydrogenation of **1**. Thus, Ni-**ZPB** was considered to be a renewable molecular flask and an efficient catalyst to promote the hydrogenation. Under saturated reaction conditions, **1** in high concentration ($K_{ass}[\mathbf{1}]^2 > 100$) exhibited pseudo zero-order kinetics of the product formation. When the concentrations of $Na_2S_2O_3$ and Ni-**ZPB** were fixed, the initial turnover frequency (TOF) of the hydrogenation reaction did not change as the substrate concentration decreased (Figure 2a and the Supporting Information, Figure S19). When the concentrations of $Na_2S_2O_3$ and **1** were fixed, the initial rate constant for hydrogenation exhibited a linear relationship with the concentration of Ni-**ZPB** (Figure 2b and the Supporting Information, Figure S20). The catalytic behavior is a Michaelis–Menten mechanism, and the rate of the reaction depends on the concentration of the host–guest species, rather than the concentration of the substrates.

To determine whether the hydrogenation reaction occurred inside the pocket of Ni-**ZPB** or outside, adenosine triphosphate (ATP), an important compound in natural systems that is inactive toward hydrogenation, was chosen as an inhibitor.[19] The microcalorimetric titration curve generated for Ni-**ZPB** upon addition of ATP revealed the formation of a host–guest system. The higher ΔH (5.7 ± 0.4 kJ mol^{-1}) and $T\Delta S$ (36.4 kJ mol^{-1}) changes compared to those of the Ni-**ZPB**/**1** system suggested that ATP was able to

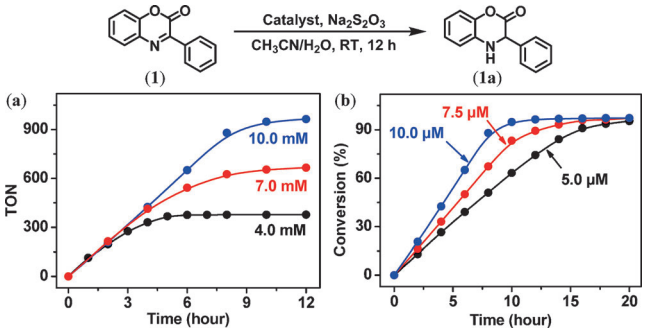

Figure 2. Kinetics of the hydrogenation reaction in the Ni-**ZPB**/**1**/$Na_2S_2O_3$ system, showing a) the variation in turnover number (per mole of the molecule Ni-**ZPB**) as the concentration of substrate **1** varies in the system containing $Na_2S_2O_3$ (50.0 mM), $\mathbf{H_2A}$ (0.10 M), and Ni-**ZPB** (10.0 μM) and b) the conversion of substrate **1** (10.0 mM) as the concentration of Ni-**ZPB** varies in the system containing $Na_2S_2O_3$ (50.0 mM) and $\mathbf{H_2A}$ (0.10 M).

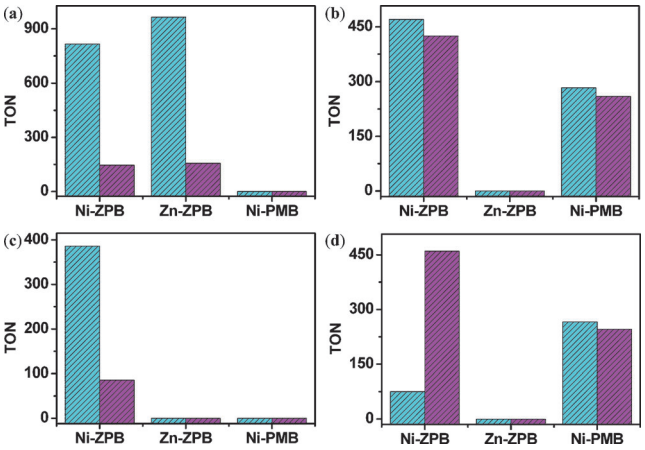

Figure 3. Turnover number per mole of the catalyst in a) the hydrogenation of substrate **1** (10.0 mM) in a system containing $Na_2S_2O_3$ (50.0 mM), $\mathbf{H_2A}$ (0.10 M), and catalyst (10.0 μM) and b) the hydrogen production in a system containing $Ru(bpy)_3^{2+}$ (1.0 mM), $\mathbf{H_2A}$ (0.10 M), and catalyst (10.0 μM). Turnover number per mole of the catalyst in c) the hydrogenation of substrate **1** (4.0 mM) and d) the hydrogen production in systems containing $Ru(bpy)_3^{2+}$ (1.0 mM), $\mathbf{H_2A}$ (0.10 M), and catalysts (10.0 μM) in one-pot transformations. The magenta and cyan bars show the absence and presence of **ATP** (20.0 mM), respectively.

replace substrate **1** and become encapsulated in the pocket of macrocycle. Upon addition of ATP to the reaction mixture, the observed decrease in the turnover number (TON) from 820 to 140 confirmed that hydrogenation occurred within the pocket of Ni-**ZPB**.[20] From a mechanistic viewpoint, the encapsulation of the substrate into the pocket forced the active sites into close proximity with substrate, enabling the hydrogenation to occur efficiently and producing the NAD^+ mimics. The product was driven out of the inner space of the pocket by the fresh substrate molecules through an equilibrium-controlled, guest-exchange reaction, and the active sites in the NADH mimics were regenerated by $Na_2S_2O_3$ for another transformation cycle. Direct microcalorimetric titration of Ni-**ZPB** upon addition of product **1a** gave ΔH and $T\Delta S$ values of -0.05 ± 0.01 and 22.8 kJ mol^{-1}, respectively for the host–guest complexation species. The fact that the free energy change (ΔG) was 7.3 kJ mol^{-1} smaller than that of **1** supported the idea that molecules of substrate **1** were able to replace product **1a** to form more stable supramolecular species, suggesting that the substrate and Ni-**ZPB** are in equilibrium with the substrate/Ni-**ZPB** complex.[21]

The cyclic voltammogram of Ni-**ZPB** demonstrated that the Ni^{II}/Ni^{I} and Ni^{I}/Ni^{0} reduction processes occurred at -0.85 V and -1.08 V (versus Ag/AgCl), respectively.[22] These potentials were within the range of the proton reduction process (Supporting Information, Figure S16), indicating the possibility of a redox-active Ni-**ZPB** catalyzing proton reduction in aqueous systems. To localize the photoinduced electron transfer and the proton reduction reaction outside the pocket, $Ru(bpy)_3^{2+}$ ions, with two positive charges and a molecular size that is larger than the inner space of the pocket in Ni-**ZPB**, were selected as the photosensitizer. Under the optimized conditions, 0.53 mL of hydrogen (TON of ca. 470 per mole of molecule Ni-**ZPB**) was generated after irradiation of a solution (5.0 mL) containing $Ru(bpy)_3^{2+}$ (1.0 mM), $\mathbf{H_2A}$ (0.10 M, ensuring that the reaction occurred under stable reductive conditions) and Ni-**ZPB** (4.0 μM) (Figure 3b and the Supporting Information, Figure S12). As expected, the addition of ATP up to 20.0 mM did not affect the efficiency of the photocatalytic hydrogen evolution (Figure 3b). The location of the hydrogenation reaction in the inner space of the pocket and the photoinduced electron transfer outside the pocket of Ni-**ZPB** provide a new approach that combines two chemical reactions in a one-pot conversion.

For comparison, the analogous Zn-**ZPB**, with redox-inactive zinc ions, and Ni-**PMB** (Figure 1b), with similar structural features except for a benzene ring substituted at the active site of the NADH model, were designed and prepared. Control experiments consisting of an identical amount of the redox-inactive Zn-**ZPB** did not produce any hydrogen under the same photocatalytic experimental conditions, and loading an identical amount of the reference compound Ni-**PMB** produced 0.32 mL of hydrogen (TON of ca. 280 per mole of Ni-**PMB**) (Figure 3b and the Supporting Information, Figure S14). Clearly, the redox-active nickel ions in our system are dominant factors in catalyzing the proton reduction under irradiation. ESI-MS spectra of Zn-**ZPB** and Ni-**PMB** solutions containing **1** exhibited new peaks at $m/z = 956.56$ and 1262.27, respectively (Supporting Information, Figures S4 and S5). These peaks are assigned to $[Zn_4(\mathbf{ZPB})(H\mathbf{ZPB})_3(\mathbf{1})_2]^{3+}$ and $[Ni_4(\mathbf{PMB})_2(H\mathbf{PMB})_2(\mathbf{1})_2]^{2+}$ ions, respectively, suggesting the possible formation of complexation species in the reaction mixture. Loading an identical amount of the analogous Zn-**ZPB** resulted in the same catalytic efficiency, 95% conversion of substrate **1**, and 15% conversion of substrate **2**. The absence of active sites in Ni-**PMB** prevents any possibility of hydrogenation transformation (Supporting Information, Figure S18).

A simple comparison of the kinetic behavior between the hydrogenation reaction with $Na_2S_2O_3$ and the light-driven hydrogen evolution revealed that the redox-inactive Zn-**ZPB** did not produce any hydrogen under the reaction conditions but was able to accelerate the hydrogenation reaction within

its pocket because of the presence of the active sites of the NADH mimics. The redox-active Ni-**PMB** could reduce protons to produce hydrogen under irradiation under the experimental conditions but could not promote the hydrogenation reaction because of the absence of the active sites of the NADH mimics. Only the redox-active Ni-**ZPB** with NADH mimic active sites could be used to catalyze the two different kinds of transformations (Figure 3a,c).

In a simple model reaction, substrate **1** (4.0 mM) was added to a solution containing $Ru(bpy)_3^{2+}$ (1.0 mM), **H_2A** (0.10 M), and Ni-**ZPB** (10.0 μM, 0.25% mol ratio of substrate **1**), and a 97% yield of the hydrogenation product was achieved (TON of ca. 390 per mole of molecule Ni-**ZPB**) (Figure 3c). Concurrently, a quite lower volume of hydrogen (0.09 mL, TON of ca. 80 per mole of molecule Ni-**ZPB**) was generated. The total turnover number for both reactions reached 470 moles per mole of Ni-**ZPB**. Upon the addition of up to 20.0 mM ATP, the hydrogenation reaction of the Ni-**ZPB**/**1**/$Ru(bpy)_3^{2+}$ system stopped, while the hydrogen evolution reaction recovered. The volume of hydrogen generated reached the same value (0.53 mL) as that in the aforementioned Ni-**ZPB**/$Ru(bpy)_3^{2+}$ system (Figure 3d). These results confirm that the addition of ATP as an inhibitor only stopped the hydrogenation reaction that occurred in the inner space of the pocket but did not quench the light-driven hydrogen evolution that occurred outside the pocket of Ni-**ZPB**. Control experiments showed that loading an identical amount of the redox-inactive Zn-**ZPB** in the same combined reactions resulted in little conversion to the hydrogenation product, and no hydrogen was detected during the reaction because the system did not produce hydrogen gas or active H-atoms for regeneration of the active sites of the hydrogenation catalyst. Loading an identical amount of Ni-**PMB** did not yield any detectable hydrogenation products but produced up to 0.30 mL of hydrogen, which was similar to the amount produced by the Ni-**PMB**/$Ru(bpy)_3^{2+}$ system under the same conditions. Upon addition of up to 20.0 mM ATP, the volume of hydrogen produced by the Ni-**PMB**/**1**/$Ru(bpy)_3^{2+}$ system did not change, and no detectable hydrogenation product was observed because the Ni-**PMB**/**1**/$Ru(bpy)_3^{2+}$ system did not contain the active sites of the hydrogenation catalyst.

When the concentrations of $Ru(bpy)_3^{2+}$ and Ni-**ZPB** were fixed, the initial TOF of the hydrogenation reaction did not vary, even if the concentration of substrate **1** was changed significantly (Figure 4a and the Supporting Information, Figure S21). In contrast, the maximum turnover number for the hydrogenation exhibits a linear relationship with the concentration of substrate **1**. The fixed initial turnover frequency with varied concentrations of substrate **1** suggests that the kinetic rate of the hydrogenation reaction depends on the concentration of the host–guest species rather than the substrate concentration. When the concentration of substrate **1** was fixed, the initial turnover frequency of the hydrogenation reaction exhibited a linear relationship with the concentration of Ni-**ZPB** (Figure 4b and the Supporting Information, Figure S22). The superiority of such combined systems that use clean energy to promote the hydrogenation

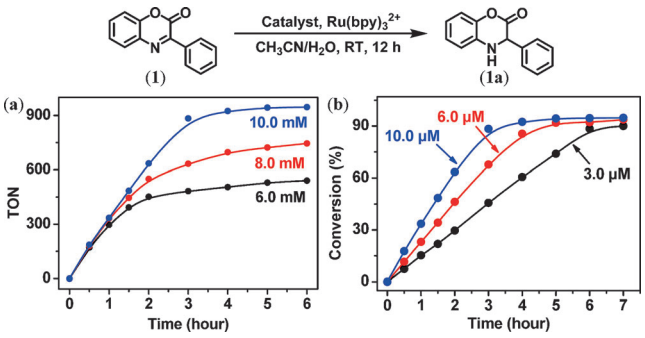

Figure 4. a) Turnover number (per mole of the molecule Ni-**ZPB**) for the hydrogenation of substrate **1** at different concentrations by the system containing $Ru(bpy)_3^{2+}$ (1.0 mM), **H_2A** (0.10 M), and Ni-**ZPB** (10.0 μM). b) Conversion in the hydrogenation of substrate **1** (10.0 mM) by the system containing $Ru(bpy)_3^{2+}$ (1.0 mM), **H_2A** (0.10 M), and different concentrations of Ni-**ZPB**.

Table 1: Conversion in the hydrogenation of substituted benzoxazinones and quinoxalinones under light irradiation.[a]

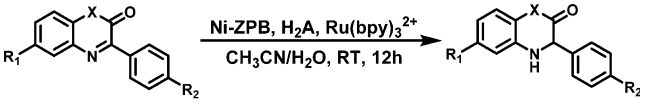

Benzoxazinone: X = O; Quinoxalinone: X = N

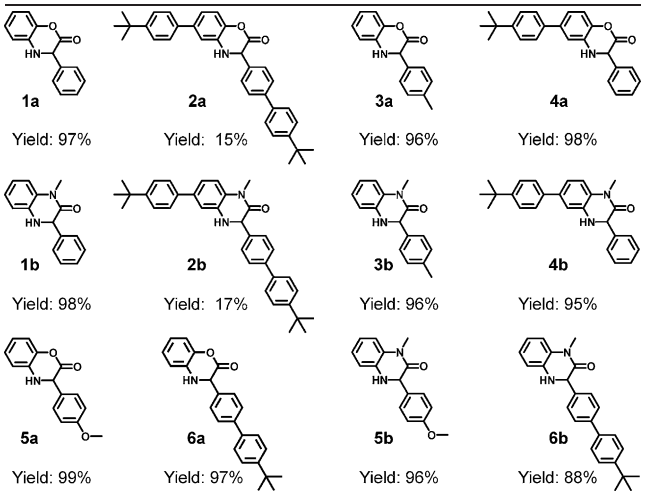

[a] Reaction conditions: substrate (4.0 mM), Ni-**ZPB** (10.0 μM), $Ru(bpy)_3^{2+}$ (1.0 mM), and **H_2A** (0.10 M) in CH_3CN/H_2O solution (1:1 v/v, pH 4.50), 12 h. The conversions were determined by ^{1}H-NMR analysis of the crude products.

reaction could be extended to several types of benzoxazinones and quinoxalinones (Table 1).

From a mechanistic viewpoint, the modified pocket of Ni-**ZPB** first encapsulates substrate **1**. The host–guest system enforces close contact between the active sites of the NADH model and the encapsulated substrate molecule. The hydrogenation reaction is localized in the inner space of the molecular flask to give the hydrogenation product and the NAD^+ mimics. At the same time, the excited state of the photosensitizer is positioned outside the flask, reducing the redox-active catalyst to give active H-atoms for the in situ regeneration of the active sites of the hydrogenation reagent

for another cycle of the hydrogenation reaction. This new synthetic platform that restricts the location of tandem redox events to the inner and outer spaces of a molecular flask renders a regenerating system that exhibits high efficiency in the light-driven hydrogenation of benzoxazinones and quinoxalinones.

Acknowledgements

This work was supported by the NSFC (No. 21501019, 21531001, and 21421005) and CPSF (No. 2014M561220).

Conflict of interest

The authors declare no conflict of interest.

Keywords: biomimetic hydrogenation · molecular flasks · proton reduction · renewable active sites · supramolecular chemistry

[1] a) C. J. Brown, F. D. Toste, R. G. Bergman, K. N. Raymond, *Chem. Rev.* **2015**, *115*, 3012 – 3035; b) K. Yan, M. Fujita, *Science* **2015**, *350*, 1165 – 1166; c) R. J. Hooley, *Nat. Chem.* **2016**, *8*, 202 – 204.

[2] a) T. K. Hyster, L. Knörr, T. R. Ward, T. Rovis, *Science* **2012**, *338*, 500 – 503; b) D. M. Kaphan, M. D. Levin, R. G. Bergman, K. N. Raymond, F. D. Toste, *Science* **2015**, *350*, 1235 – 1238.

[3] a) Q. Q. Wang, S. Gonell, S. H. A. M. Leenders, M. Dürr, I. Ivanović-Burmazović, J. N. H. Reek, *Nat. Chem.* **2016**, *8*, 225 – 230; b) T. R. Cook, P. J. Stang, *Chem. Rev.* **2015**, *115*, 7001 – 7045.

[4] a) X. Jing, C. He, Y. Yang, C. Y. Duan, *J. Am. Chem. Soc.* **2015**, *137*, 3967 – 3974; b) D. Kim, D. R. Whang, S. Y. Park, *J. Am. Chem. Soc.* **2016**, *138*, 8698 – 8701.

[5] a) X. Y. Dong, M. Zhang, R. B. Pei, Q. Wang, D. H. Wei, S. Q. Zang, Y. T. Fan, T. C. W. Mak, *Angew. Chem. Int. Ed.* **2016**, *55*, 2073 – 2077; *Angew. Chem.* **2016**, *128*, 2113 – 2117; b) X. J. Kong, Z. Lin, Z. M. Zhang, T. Zhang, W. B. Lin, *Angew. Chem. Int. Ed.* **2016**, *55*, 6411 – 6416; *Angew. Chem.* **2016**, *128*, 6521 – 6526.

[6] a) P. A. Frey, *Science* **2001**, *294*, 2489 – 2490; b) E. Purwantinia, B. Mukhopadhyay, *Proc. Natl. Acad. Sci. USA* **2009**, *106*, 6333 – 6338.

[7] a) B. G. Caulkins, B. Bastin, C. Yang, T. J. Neubauer, R. P. Young, E. Hilario, Y. M. Huang, C. A. Chang, L. Fan, F. Dunn, M. M. J. Marsella, L. J. Mueller, *J. Am. Chem. Soc.* **2014**, *136*, 12824 – 12827; b) M. D. White, K. A. P. Payne, K. Fisher, S. A. Marshall, D. Parker, N. J. W. Rattray, D. K. Trivedi, R. Goodacre, S. E. J. Rigby, N. S. Scrutton, S. Hay, D. Leys, *Nature* **2015**, *522*, 502 – 506.

[8] a) S. Betanzos-Lara, Z. Liu, A. Habtemariam, A. M. Pizarro, B. Qamar, P. J. Sadler, *Angew. Chem. Int. Ed.* **2012**, *51*, 3897 – 3900; *Angew. Chem.* **2012**, *124*, 3963 – 3966; b) T. Knaus, C. E. Paul, C. W. Levy, S. de Vries, F. G. Mutti, F. Hollmann, N. S. Scrutton, *J. Am. Chem. Soc.* **2016**, *138*, 1033 – 1039.

[9] a) Q. A. Chen, M. W. Chen, C. B. Yu, L. Shi, D. S. Wang, Y. Yang, Y. G. Zhou, *J. Am. Chem. Soc.* **2011**, *133*, 16432 – 16435; b) V. Köhler, Y. M. Wilson, M. Dürrenberger, D. Ghislieri, E. Churakova, T. Quinto, L. Knörr, D. Häussinger, F. Hollmann, N. J. Turner, T. R. Ward, *Nat. Chem.* **2013**, *5*, 93 – 99.

[10] a) Y. Maenaka, T. Suenobu, S. Fukuzumi, *J. Am. Chem. Soc.* **2012**, *134*, 367 – 374; b) Q. A. Chen, K. Gao, Y. Duan, Z. S. Ye, L. Shi, Y. Yang, Y. G. Zhou, *J. Am. Chem. Soc.* **2012**, *134*, 2442 – 2448; c) L. Q. Lu, Y. H. Li, K. Junge, M. Beller, *Angew. Chem. Int. Ed.* **2013**, *52*, 8382 – 8386; *Angew. Chem.* **2013**, *125*, 8540 – 8544.

[11] a) Y. Okamoto, V. Köhler, T. R. Ward, *J. Am. Chem. Soc.* **2016**, *138*, 5781 – 5784; b) A. McSkimming, S. B. Colbran, *Chem. Soc. Rev.* **2013**, *42*, 5439 – 5488; c) C. Zheng, S. L. You, *Chem. Soc. Rev.* **2012**, *41*, 2498 – 2518.

[12] a) W. T. Eckenhoff, R. Eisenberg, *Dalton Trans.* **2012**, *41*, 13004 – 13021; b) Z. Han, R. Eisenberg, *Acc. Chem. Res.* **2014**, *47*, 2537 – 2544.

[13] Z. He, C. He, Z. M. Wang, E. Q. Gao, Y. Liu, C. H. Yan, *Dalton Trans.* **2004**, 502 – 504.

[14] a) Y. Ferrand, M. P. Crump, A. P. Davis, *Science* **2007**, *318*, 619 – 622; b) Y. Z. Liu, C. H. Hu, A. Comotti, M. D. Ward, *Science* **2011**, *333*, 436 – 440.

[15] a) N. Chandramouli, Y. Ferrand, G. Lautrette, B. Kauffmann, C. D. Mackereth, M. Laguerre, D. Dubreuil, I. Huc, *Nat. Chem.* **2015**, *7*, 334 – 341; b) M. Yoshizawa, M. Tamura, M. Fujita, *Science* **2006**, *312*, 251 – 254.

[16] C. Zhang, S. Li, C. Zhang, Y. Liu, *Org. Biomol. Chem.* **2015**, *13*, 10808 – 10812.

[17] J. W. Liu, L. F. Chen, H. Cui, J. Y. Zhang, L. Zhang, C. Y. Su, *Chem. Soc. Rev.* **2014**, *43*, 6011 – 6061.

[18] a) T. McKee, J. R. McKee, *Biochemistry: The Molecular Basis of Life*, 3rd ed., McGraw-Hill, New York, **2003**; b) R. Breslow, *Acc. Chem. Res.* **1991**, *24*, 159 – 164.

[19] C. He, J. Wang, L. Zhao, T. Liu, J. Zhang, C. Y. Duan, *Chem. Commun.* **2013**, *49*, 627 – 629.

[20] a) S. M. Biros, R. M. Yeh, K. N. Raymond, *Angew. Chem. Int. Ed.* **2008**, *47*, 6062 – 6064; *Angew. Chem.* **2008**, *120*, 6151 – 6153; b) C. J. Hastings, D. Fiedler, R. G. Bergman, K. N. Raymond, *J. Am. Chem. Soc.* **2008**, *130*, 10977 – 10983.

[21] a) H. C. Lo, R. H. Fish, *Angew. Chem. Int. Ed.* **2002**, *41*, 478 – 481; *Angew. Chem.* **2002**, *114*, 496 – 499; b) B. Procuranti, S. J. Connon, *Chem. Commun.* **2007**, 1421 – 1423.

[22] E. S. Wiedner, H. J. S. Brown, M. L. Helm, *J. Am. Chem. Soc.* **2016**, *138*, 604 – 616.

Manuscript received: March 21, 2017
Revised manuscript received: May 15, 2017
Version of record online: ■■ ■■, ■■■■

Communications

Host–Guest Systems

L. Zhao, J. Wei, J. Lu, C. He,*
C. Duan* ——— ■■■■–■■■■

Renewable Molecular Flasks with NADH Models: Combination of Light-Driven Proton Reduction and Biomimetic Hydrogenation of Benzoxazinones

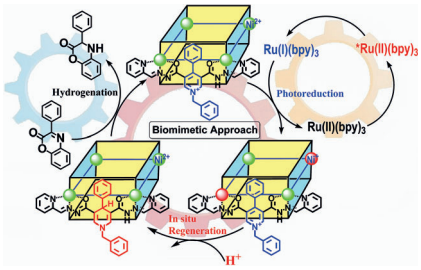

In the pocket: Through modulation of the active sites of NADH models in redox-active molecular flasks, a new synthetic platform that controls the location of biomimetic hydrogenation and in situ photocatalytic proton reduction to the inner and outer spaces of the pocket, respectively, was developed that echoes the properties of enzymes for the one-pot transformation of benzoxazinones and quinoxalinones using light as a clean energy source.